



Cite this: *Chem. Sci.*, 2020, **11**, 2796

All publication charges for this article have been paid for by the Royal Society of Chemistry

The duality of electron localization and covalency in lanthanide and actinide metallocenes[†]

Danil E. Smiles,^a Enrique R. Batista,^{†,b} Corwin H. Booth,^a David L. Clark,^b Jason M. Keith,^{†,c} Stosh A. Kozimor,^{†,b} Richard L. Martin,^b Stefan G. Minasian,^{†,a} David K. Shuh,^{†,a} S. Chantal E. Stieber,^{†,d} and Tolek Tyliszczak^a

Previous magnetic, spectroscopic, and theoretical studies of cerocene, $\text{Ce}(\text{C}_8\text{H}_8)_2$, have provided evidence for non-negligible 4f-electron density on Ce and implied that charge transfer from the ligands occurs as a result of covalent bonding. Strong correlations of the localized 4f-electrons to the delocalized ligand π -system result in emergence of Kondo-like behavior and other quantum chemical phenomena that are rarely observed in molecular systems. In this study, $\text{Ce}(\text{C}_8\text{H}_8)_2$ is analyzed experimentally using carbon K-edge and cerium $M_{5,4}$ -edge X-ray absorption spectroscopies (XAS), and computationally using configuration interaction (CI) calculations and density functional theory (DFT) as well as time-dependent DFT (TDDFT). Both spectroscopic approaches provide strong evidence for ligand \rightarrow metal electron transfer as a result of Ce 4f and 5d mixing with the occupied C 2p orbitals of the $\text{C}_8\text{H}_8^{2-}$ ligands. Specifically, the Ce $M_{5,4}$ -edge XAS and CI calculations show that the contribution of the $4f^1$, or Ce^{3+} , configuration to the ground state of $\text{Ce}(\text{C}_8\text{H}_8)_2$ is similar to strongly correlated materials such as CeRh_3 and significantly larger than observed for other formally Ce^{4+} compounds including CeO_2 and CeCl_6^{2-} . Pre-edge features in the experimental and TDDFT-simulated C K-edge XAS provide unequivocal evidence for C 2p and Ce 4f covalent orbital mixing in the δ -antibonding orbitals of e_{2u} symmetry, which are the unoccupied counterparts to the occupied, ligand-based δ -bonding e_{2u} orbitals. The C K-edge peak intensities, which can be compared directly to the C 2p and Ce 4f orbital mixing coefficients determined by DFT, show that covalency in $\text{Ce}(\text{C}_8\text{H}_8)_2$ is comparable in magnitude to values reported previously for $\text{U}(\text{C}_8\text{H}_8)_2$. An intuitive model is presented to show how similar covalent contributions to the ground state can have different impacts on the overall stability of f-element metallocenes.

Received 3rd December 2019
Accepted 4th February 2020

DOI: 10.1039/c9sc06114b
rsc.li/chemical-science

Introduction

Since the discovery of cerocene, $\text{Ce}(\text{C}_8\text{H}_8)_2$,^{1,2} a broad debate has ensued regarding the true nature of f-element chemical bonds, the meaning of terms used to describe bonding, and how and when those terms should be used. In the ionic limit, balancing the charges of two dianionic cyclooctatetraene ligands ($\text{C}_8\text{H}_8^{2-}$) requires that the cerium atom have a formal +4 charge which leaves the 4f and 5d orbitals unoccupied. This model is supported by a structural analysis of $\text{Ce}(\text{C}_8\text{H}_8)_2$ and comparison with other lanthanocenes and actinocenes.^{3–7} The

diamagnetic NMR spectrum^{8,9} of $\text{Ce}(\text{C}_8\text{H}_8)_2$ and similarities between the photoelectron spectra^{2,10,11} of $\text{Ce}(\text{C}_8\text{H}_8)_2$ and $\text{Th}(\text{C}_8\text{H}_8)_2$ seem to support a Ce^{4+} formulation, although subsequent theoretical analyses¹² provide a more nuanced interpretation. In the 1990s, $\text{Ce}(\text{C}_8\text{H}_8)_2$ was among the first systems to be the focus of computational studies utilizing configuration interaction concepts to account for electron-electron interactions.^{12–14} These studies find that the ground state electronic configuration of $\text{Ce}(\text{C}_8\text{H}_8)_2$ is a mixture of two different configurations, and that $\text{Ce}(\text{C}_8\text{H}_8)_2$ is best approximated as a predominantly Ce^{3+} ($4f^1$) compound together with two $\text{C}_8\text{H}_8^{1,5-}$ ligands. The possibility of a multiconfigurational ground state has been explored extensively with theory, and more recent computational studies expand on this interpretation by providing additional strong support for a non-negligible 4f orbital occupation in the ground state of $\text{Ce}(\text{C}_8\text{H}_8)_2$.^{15–17} Experimental corroboration has been more difficult to obtain, however, and it is difficult to rationalize the apparent contradictions in between previous measurements^{9,18–20} which suggest that the 4f-electrons participate in

^aLawrence Berkeley National Laboratory, Berkeley, California 94720, USA. E-mail: sgminasian@lbl.gov

^bLos Alamos National Laboratory, Los Alamos, New Mexico 87545, USA. E-mail: erbatista@lanl.gov

^cColgate University, Hamilton, New York 13346, USA

^dCalifornia State Polytechnic University, Pomona, California 91768, USA. E-mail: sesieber@cpp.edu

[†] Electronic supplementary information (ESI) available: Additional plots and tabulated data. See DOI: [10.1039/c9sc06114b](https://doi.org/10.1039/c9sc06114b)



bonding while appearing localized simultaneously. Cerium L₃-edge measurements²⁰ of Ce(C₈H₈)₂ provide the only direct experimental evidence of a multiconfigurational ground state, but the spectral interpretations are fraught with controversy.^{21–24} Taken together, these studies have raised more basic questions regarding whether the concept of a multiconfigurational ground state should apply to all f-element compounds, how it equates to more established models of metal-ligand covalency,²⁵ and how it is manifested by changes in chemical reactivity or magnetic behavior. Although Ce(C₈H₈)₂ is prototypical, such fundamental questions pertain to all formal Ce⁴⁺ compounds^{26–35} and high valent lanthanide compounds,^{36–41} ytterbium complexes,^{42–48} and the transuranic actinocenes^{15,17,49} and have implications throughout the periodic table for the electronic structure models used to describe bonding near the limits of chemically accessible oxidation states.^{50,51} Improved theoretical models of bonding in these systems are needed to develop new ligands and innovative concepts in lanthanide/actinide separations for nuclear energy.⁵² Efforts to unravel the complex behavior of correlated electron systems also benefit from investigations of self-contained phenomena in single molecules that can be more precisely characterized using spectroscopy and theory.^{53–60}

Our recent work has shown that the metal-ligand covalency and multiconfigurational ground states can be probed experimentally in f-element coordination compounds with X-ray absorption spectroscopy, XAS, at the K-edges for the light atoms directly bound to metal centers (collectively referred to as ligand K-edge XAS).^{61–64} The spectroscopic technique probes bound state transitions of core 1s electrons localized on the ligands to unoccupied molecular orbitals, which only have intensity if the final state orbitals have ligand np character (n = principal quantum number). Through a combination of ligand K-edge XAS and time-dependent density functional theory (TDDFT) calculations, Solomon and coworkers provided the first demonstrations of this approach as a direct and quantitative probe of electronic structure and covalent bonding in transition metal complexes with M-Cl and M-S bonds.^{65–68} Recently, the range of ligand chemistries was expanded to include systems incorporating M-O,^{69–71} M-N,^{72–74} and M-C bonds.^{75,76} By acquiring XAS using a scanning transmission X-ray microscope (STXM), we are able to control saturation effects and overcome other challenges with photon attenuation that can preclude measurements with weakly penetrating incident radiation using soft X-rays. Herein, we examine 4f-electron localization in Ce(C₈H₈)₂ using DFT and C K-edge XAS from STXM. Unambiguous evidence for covalent mixing involving the 4f orbitals of e_{2u} symmetry is identified in the experimental spectra with the aid of TDDFT calculations. The results are interpreted in the context of Ce M_{5,4}-edge XAS and multiplet calculations, which also show that Ce(C₈H₈)₂ has significant covalent character owing to ligand-to-metal electron transfer in the ground state. Both molecular orbital theory and configuration interaction models are presented to rationalize these observations relative to earlier work on the actinocenes, and we show how the 4f-electrons

can participate in bonding while appearing localized simultaneously.

Results and discussion

Ground state electronic structure and molecular orbital description

A framework for understanding the C K-edge and Ce M_{5,4}-edge spectra of Ce(C₈H₈)₂ can be approximated using molecular orbital (MO) theory following conventions developed for actinide systems, particularly U(C₈H₈)₂.²⁵ In a D_{8h} ligand field, the shape and symmetry of ligand orbitals that are involved in M-C bonding can be estimated from symmetry adapted linear combinations (SALCs) of the sixteen atomic C 2p π orbitals that are perpendicular to the ring planes (C-C π bonding). In this scheme, the centrosymmetric Ce 5d orbitals mix with the C 2p SALCs of a_{1g} (5d- σ), e_{1g} (5d- π), and e_{2g} (5d- δ) symmetry while the Ce 4f orbitals can mix with the a_{2u} (4f- σ), e_{1u} (4f- π), e_{2u} (4f- δ), and e_{3u} (4f- ϕ) SALCs, which leaves the SALCs of b_{1g} + b_{2g} + e_{3g} symmetries non-bonding. Many previous spectroscopic^{11,75,77,78} and theoretical^{10,15–17,49,79,80} studies of f-element metallocenes show that f-orbital mixing is dominated by the δ -bonding MOs of e_{2u} symmetry when compared with the σ , π , and ϕ -bonding MOs. Mixing in the e_{2u} orbitals in Ce(C₈H₈)₂ is described using the MO model by the linear combination of orbitals as:

$$\Psi(e_{2u}) = N\{4f - \lambda\pi_{e2u}\} \quad (1)$$

where N is a normalization constant, λ is the mixing coefficient, and 4f and π_{e2u} are parent Ce and ligand-based wavefunctions. In eqn (1), λ is given by

$$\lambda = H/[E^0(4f) - E^0(\pi_{e2u})] \quad (2)$$

where the term $E^0(4f) - E^0(\pi_{e2u})$ is the difference in energy between the 4f and π_{e2u} wavefunctions and H is the off-diagonal Hamiltonian matrix element, which is proportional to the overlap integral. The dominance of e_{2u} bonding is easily understood by eqn (2), wherein a larger λ results from a better energy match between the 4f-based e_{2u} orbitals and the high energy e_{2u} SALCs (small $E^0(4f) - E^0(\pi_{e2u})$),²⁵ and also to more directional δ -bonds resulting in better orbital overlap (large H).^{78,81} However, large values of λ are not necessarily correlated with large stabilizations due to covalency because the energetic stabilization has a greater dependence on orbital overlap:

$$\Delta E = H^2/[E^0(4f) - E^0(\pi_{e2u})] = H\lambda \quad (3)$$

As will be shown below, and also described previously,^{62,82–84} the lack of significant f-orbital overlap can result in a counterintuitive relationship between stability and f-orbital covalency for many lanthanide and actinide compounds.

Ground state DFT calculations with the B3LYP hybrid functional were conducted on the closed shell configuration to guide assignments of the experimental spectra. The unoccupied orbitals relevant to the C K-edge XAS measurements are summarized in Table 1 and Fig. 1. Similar to results from DFT calculations on Th(C₈H₈)₂ and U(C₈H₈)₂,⁷⁵ inspection of the



Table 1 Calculated energies^a and atomic compositions^b of selected virtual molecular orbitals for Ce(C₈H₈)₂

Orbital	Energy (eV)	MO (DFT)					
		C 2s	C 2p	M 4f	M 5d	M 6s	M 6p
1b _{2g} (Ce-C nb)	4.57	0	0.98	0	0	0	0
1b _{1u} (Ce-C nb)	4.23	0	0.96	0	0	0	0
2e _{1g} (5d- π)	2.25	-0.15	0.14	0	0.63	0	0
2e _{2g} (5d- δ)	1.78	-0.01	0.22	0	0.76	0	0
1e _{3g} (Ce-C nb)	1.37	0	0.96	0	0	0	0
2e _{3u} (4f- ϕ)	1.09	0	0.89	0.07	0	0	0
2a _{1g} (5d- σ)	-0.82	0.02	0.02	0	0.77	0.06	0
2e _{1u} (4f- π)	-1.77	0	0.00	0.98	0	0.01	0
1e _{3u} (4f- ϕ)	-1.84	0	0.05	0.95	0	0	0
2e _{2u} (4f- δ)	-1.85	0	0.24	0.76	0	0	0
2a _{2u} (4f- σ)	-2.01	0	0.02	0.98	0	0	0

^a Alpha spin-orbital energies are reported. ^b The use of a non-orthogonal basis set can cause Mulliken analysis to have nonphysical results such as compositions >100%, or <0.⁸⁵ The lowest energy MOs are the antibonding LUMO.

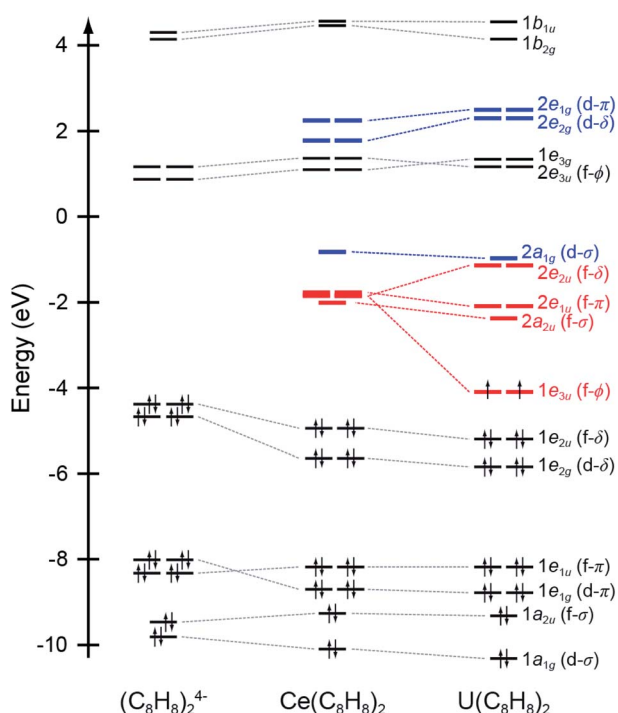


Fig. 1 Quantitative molecular orbital diagram showing DFT calculated energies for Ce(C₈H₈)₂ relative to those published previously for U(C₈H₈)₂ and an idealized (C₈H₈)⁴⁻ fragment in D_{4h} symmetry.⁷⁵ Energies for the (C₈H₈)⁴⁻ fragment have been shifted by -16.42 eV so that the carbon 1s orbital energies match those of U(C₈H₈)₂.

Mulliken population analysis for Ce(C₈H₈)₂ in Table 1 shows that the molecular orbitals of e_{2u} (4f- δ) symmetry played a significant role in bonding with the C₈H₈²⁻ ligands, while the orbitals of a_{2u} (4f- σ) and e_{1u} (4f- π) symmetry were best described as metal-based orbitals having negligible C 2p character. In contrast to Th(C₈H₈)₂, where 5f ϕ -bonding was an important part of the valence electronic structure,⁷⁵ Ce(C₈H₈)₂

more closely resembled U(C₈H₈)₂ in that the $1e_{3u}$ and $2e_{3u}$ orbitals are best described as non-bonding Ce 4f and C 2p based orbitals, respectively.

DFT is advantageous because it describes partial electron delocalization due to covalency associated with specific bonding interactions (e.g., σ , π , δ , ϕ), which has proven useful for interpretation of ligand K-edge spectra.^{67,86,87} Results from the hybrid DFT closed-shell singlet approach used here agreed qualitatively with the established descriptions of Ce(C₈H₈)₂ electronic structure from SCF,^{12,13,88} hybrid DFT,⁸⁹ and multi-reference calculations,^{15,17,90} along with related calculations for the actinocenes.^{75,79,81,90-94} Alternatively, the single determinant MO wavefunction shown in eqn (1) can be reformulated using a configuration interaction (CI) charge transfer model. The CI model accounts for exchange, multiple and core-induced charge transfer interactions, which are typically difficult to incorporate, or not incorporated in MO models. In the CI model where configurations differ by only one electron, the ground state is expressed as

$$\Psi = N[|4f^0L^4\rangle + \lambda|4f^1L^3\rangle] \quad (4)$$

where the first term is the ionic configuration with a Ce⁴⁺ atom and the second configuration describes the result of a ligand-to-metal electron transfer leading to reduction to Ce³⁺.⁹⁵ Eqn (4) neglects the $4f^2L^2$ configuration, which is strongly reduced due to a Coulomb interaction between the two 4f electrons but theoretically non-zero.¹⁵ Previous theoretical work has shown that CI expansions are highly dependent on the orbital basis that is employed,¹⁵⁻¹⁷ such that this representation of λ is quantitatively different than that provided in eqn (1) and (2). However, because the electrons are assumed to be fully localized, the CI model can be directly compared to physical observables from metal-based XAS and magnetic measurements.⁹⁶ For example, Ce L₃-edge measurements of Ce(C₈H₈)₂ provided a 4f orbital occupancy, n_f , of 0.89(3) electrons, which agrees well with previously reported theoretical values which range between about 0.80 to 0.95 electrons.^{12,13,15-17} Earlier theoretical studies^{12,13,97} also used the CI model and described how the unpaired 4f¹ electron in the Ce³⁺ configuration couples with the ligand $\pi_{e_{2u}}^3$ hole to form a ground state singlet, which is analogous to the Kondo effect observed in some extended solids and intermetallics.^{98,99} Ce(C₈H₈)₂ was predicted to exhibit temperature independent paramagnetism (TIP) as a result of the Kondo effect,^{12,13,97} which was confirmed experimentally by Andersen and co-workers using SQUID magnetometry.^{9,20}

A possible concern therefore lies with the closed-shell nature of the DFT solution, which could provide an inaccurate or wholly incorrect formulation of the multiconfigurational ground-state for many-electron lanthanide and actinide systems.^{100,101} In fact, the hybrid DFT approximation can make direct contact with the multi-configuration representations by examining the B3LYP closed-shell determinant for instabilities. Preliminary calculations, which will be reported separately, indeed reveal a broken-symmetry B3LYP ground state that is nearly degenerate with the closed-shell solution described above. The broken symmetry ground state is an open-shell



singlet (an admixture of singlet and triplet states) which couples a Ce 4f electron with a hole on the ligands. When the triplet state is projected from the broken-symmetry determinant, the pure singlet state lies some 0.49 eV below the closed-shell solution,¹⁰² and provides additional evidence for an open-shell singlet ground state as inferred above. This simple broken symmetry wavefunction seems to capture much of the multi-configurational aspects of $\text{Ce}(\text{C}_8\text{H}_8)_2$ demonstrated in earlier work cited above.

STXM measurements

A scanning transmission X-ray microscope (STXM) was utilized to image and obtain C K-edge and Ce $M_{5,4}$ -edge XAS from micron-scale crystals of $\text{Ce}(\text{C}_8\text{H}_8)_2$.¹⁰³ This has been demonstrated previously^{71,75} as an effective approach for minimizing the saturation and self-absorption effects that can plague efforts to obtain spectra using weakly penetrating incident radiation at low photon energies. For samples prepared from finely-divided powders, it was necessary to identify particles that were sufficiently thin¹⁰⁴ for transmission XAS measurements and also large enough to provide a suitable signal-to-background ratio. Utilizing methodology developed for the study of group 4 bent metallocene dichlorides, $(\text{C}_5\text{H}_5)_2\text{MCl}_2$ (M = Ti, Zr, Hf)⁷⁶ and actinocenes (C_8H_8)₂An (An = Th, U),⁷⁵ small droplets of $\text{Ce}(\text{C}_8\text{H}_8)_2$ dissolved in toluene were allowed to evaporate on Si_3N_4 windows in an Ar-filled glovebox to form a large number of small crystallites in a compact area that were suitable for STXM raster scans (Fig. 2).

Initially, $\text{Ce}(\text{C}_8\text{H}_8)_2$ was found to be susceptible to radiation damage during the room-temperature STXM experiments when using standard data acquisition parameters as evidenced by rapid changes in spectral profile and by the emergence of interface distortions in images of the crystallites. To quantify contributions from radiation damage and show a progression from $\text{Ce}(\text{C}_8\text{H}_8)_2$ to the unidentified product(s) resulting from radiation damage as a function of photon exposure time, short acquisitions of C K-edge and Ce M_5 -edge spectra were performed in rapid succession over the same sample area (Fig. 3). As described previously for O K-edge measurements on light-sensitive compounds such as potassium permanganate,⁷¹ the duration of each individual scan was limited by reducing the

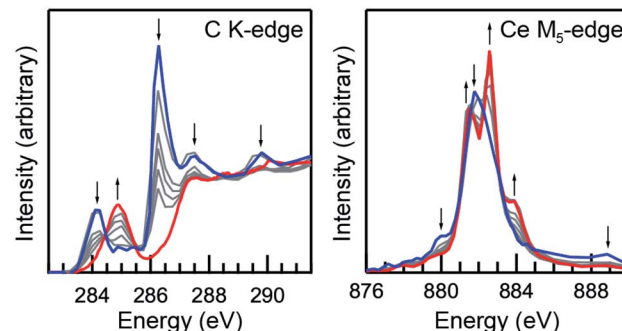


Fig. 3 Room-temperature C K-edge (left) and Ce $M_{5,4}$ -edge (right) XAS results showing a progression of increasing photon damage following repeated spectral acquisitions on a sample of $\text{Ce}(\text{C}_8\text{H}_8)_2$. Individual scan times were reduced by limiting the number of energy points per spectrum and the dwell time, and by selecting larger particles (see Experimental). The first (blue) and final (red) scan are given with several intermediate scans (gray). Arrows indicate the changes in spectral intensity with increasing damage.

number of pixels, the dwell time per pixel, and by using coarse energy step sizes (see Experimental). The product(s) resulting from radiation damage could not be rigorously identified, however, inspection of the Ce M_5 -edge following repeated scans showed a spectral profile that is characteristic of Ce^{3+} species. Spectra obtained at the beginning of these experiments (Fig. 3, blue) and before the onset of radiation damage confirm that the C K-edge and Ce $M_{5,4}$ -edge spectra described below are representative of $\text{Ce}(\text{C}_8\text{H}_8)_2$ with minimal contributions from radiation damage. High quality C K-edge and Ce $M_{5,4}$ -edge XAS were ultimately obtained by averaging datasets from more than 10 independent crystals and by selecting thin crystals (<100 nm) with a large surface area (>4 μm^2 with respect to dimensions normal to the beam).

Cerium $M_{5,4}$ -edge XAS

Ce $M_{5,4}$ -edge XAS were obtained and compared with earlier L_3 -edge XAS studies of $\text{Ce}(\text{C}_8\text{H}_8)_2$.^{20,69} The $M_{5,4}$ -edge spectroscopic approach probes electric dipole-allowed $3\text{d}^{10}4\text{f}^n \rightarrow 3\text{d}^94\text{f}^{n+1}$ transitions, where n is the number of 4f electrons in the ground state. Because $M_{5,4}$ -edge XAS probes the 4f orbitals directly, it can be advantageous for probing 4f orbital occupation and mixing in systems with multiconfigurational ground states. Fig. 4 compares the background subtracted and normalized Ce $M_{5,4}$ -edge spectra for $\text{Ce}(\text{C}_8\text{H}_8)_2$ and $[\text{Ce}(\text{C}_8\text{H}_8)_2]\text{Li}(\text{THF})_2$ together with selected reference materials CeO_2 , CeRh_3 , CeCl_6^{2-} , and CeCl_6^{3-} .^{64,69,105} Each of the spectra are split by approximately 18 eV into a M_5 -edge ($3\text{d}_{5/2} \rightarrow 4\text{f}_{7/2}$ and $3\text{d}_{5/2} \rightarrow 4\text{f}_{5/2}$) and M_4 -edge ($3\text{d}_{3/2} \rightarrow 4\text{f}_{5/2}$) because of the spin-orbit coupling with the core-hole. For CeCl_6^{3-} and $[\text{Ce}(\text{C}_8\text{H}_8)_2]\text{Li}(\text{THF})_2$, both the M_5 - and M_4 -edges exhibit energy shifts and fine structure that are characteristic of multiplet splittings observed in the Ce $M_{5,4}$ -edge spectra from other formal Ce^{3+} compounds.¹⁰⁶⁻¹⁰⁹ Likewise, the Ce $M_{5,4}$ -edge spectra for CeCl_6^{2-} , CeO_2 , CeRh_3 ,¹⁰⁵ and $\text{Ce}(\text{C}_8\text{H}_8)_2$ consist of main M_5 and M_4 peaks and weaker “satellite” features at higher energies that

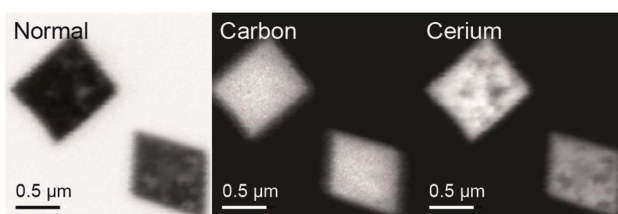


Fig. 2 Three STXM images of $\text{Ce}(\text{C}_8\text{H}_8)_2$ crystals: (from left to right) a contrast image obtained with a photon energy of 882.0 eV and elemental distribution maps obtained by subtraction using photon energies of 286.3–276.3 eV (C) and 882.0–872.0 eV (Ce). Some photon damage occurred while acquiring the high-resolution images as shown by dark spots. The crystals are representative of others which were used to obtain C K-edge and Ce $M_{5,4}$ -edge XAS data.



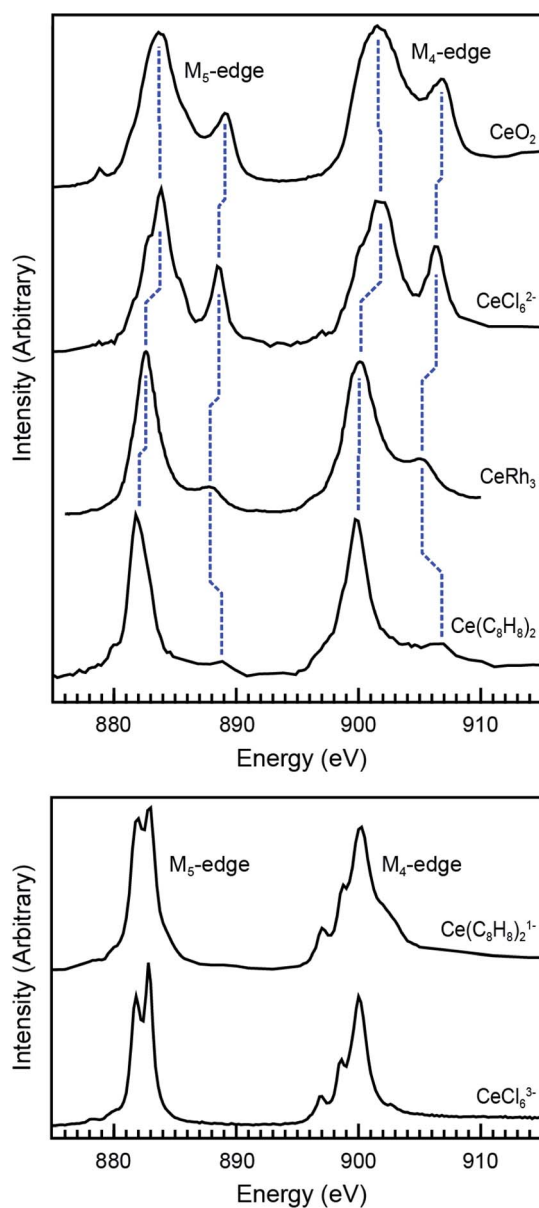


Fig. 4 Top panel: Ce M_{5,4}-edge XAS of formal Ce⁴⁺ compounds including Ce(C₈H₈)₂ and reference materials CeO₂, CeRh₃, and (Et₄N)₂CeCl₆. Bottom panel: Ce M_{5,4}-edge XAS of the formal Ce³⁺ compound [Li(THF)₂][Ce(C₈H₈)₂] and reference material (Ph₄P)₃CeCl₆. The data for CeRh₃ was reproduced using Digitizelt from ref. 105, copyright 1985 Elsevier. Data for CeO₂ was adapted with permission from ref. 69 copyright 2017 American Chemical Society. Data for (Et₄N)₂CeCl₆ and (Ph₄P)₃CeCl₆ was adapted with permission from ref. 64, copyright 2015 American Chemical Society.

are generally consistent with earlier measurements of formal Ce⁴⁺ compounds. However, closer inspection of the spectra in Fig. 4 showed that the main M_{5,4}-edge peaks for Ce(C₈H₈)₂ (882.0 and 900.0 eV) and CeRh₃ (882.6 and 900.1 eV) were found approximately 1.5 eV lower in energy than observed for CeCl₆²⁻ (883.7 and 901.6 eV) or CeO₂ (883.7 and 901.7 eV). In this regard, the main M_{5,4}-edge energies observed for Ce(C₈H₈)₂ and CeRh₃ more closely resemble those of formally Ce³⁺ compounds

including CeCl₆³⁻ (882.3 and 900.0 eV) and [Ce(C₈H₈)₂][Li(THF)₂] (882.4 and 900.2 eV). The similarity between Ce(C₈H₈)₂ and intermetallic compounds¹⁰⁵ CeRh₃ as well as CeRu₂ and CeCo₂ could be anticipated given the close correspondence between the L₃-edge spectral profiles for those compounds.^{110,111} It is worth noting that the M_{5,4}-edge XAS of Ce(C₈H₈)₂ also exhibited a 7 eV average separation between the main and satellite features, which is significantly larger than observed for CeO₂, CeCl₆²⁻, or CeRh₃ (4.8, 4.9, and 5.0 eV, respectively).

To explore these results further, CI calculations were conducted for Ce(C₈H₈)₂ and [Ce(C₈H₈)₂][Li(THF)₂]. The method was employed using the CTM4XAS program, which is a semi-empirical approach developed by de Groot and is based on Cowan's code (Fig. 5 and Table 2).¹¹²⁻¹¹⁴ The CTM4XAS approach provides an accurate calculation of the multiplet states accessible to a free Ce ion while approximating the influence of the ligands by accounting for symmetry and charge transfer. Previous calculations have reproduced the fine structure and satellite features in M_{5,4}-edge spectra of formally tetravalent

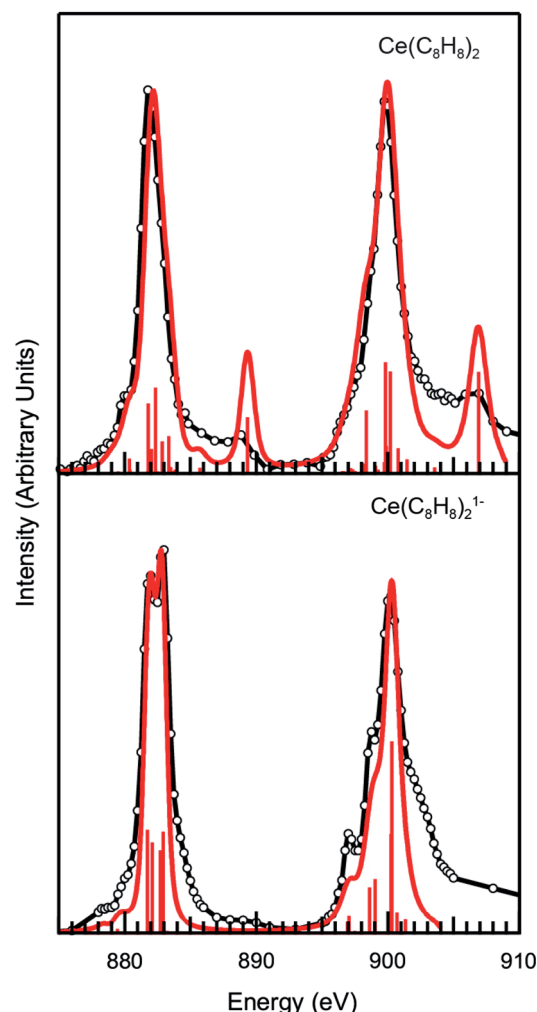


Fig. 5 Experimental Ce M_{5,4}-edge spectra (black) and CTM4XAS calculations (red) for Ce(C₈H₈)₂ and [Ce(C₈H₈)₂][Li(THF)₂].



Table 2 Comparison of the CTM4XAS calculation parameters and results for CeCl_6^{2-} ,⁶⁴ CeO_2 ,⁶⁹ and $\text{Ce}(\text{C}_8\text{H}_8)_2$. See the Experimental for additional details

	CeCl_6^{2-}	CeO_2	$\text{Ce}(\text{C}_8\text{H}_8)_2$
ΔE_{gs}	2.5 eV	2.0 eV	−0.1 eV
ΔE_{fs}	−1.5 eV	−1.8 eV	−5.0 eV
$T_{\text{gs}} = T_{\text{fs}}$	0.70	0.70	0.75
$3d^{10}4f^0$	75%	70%	49%
$3d^{10}\underline{L}4f^1$	25%	30%	51%
LMCT calc.	3.6 eV	3.2 eV	2.2 eV
LMCT exp.	3.3 eV	3.1 eV	2.1 eV

compounds including CeCl_6^{2-} and CeO_2 .^{64,69,83} This approach has also been applied successfully to model $M_{5,4}$ -edge spectra and to develop quantitative interpretations of charge transfer interactions in the ground state for other transition metal and Ce systems.^{95,115,116} For $[\text{Ce}(\text{C}_8\text{H}_8)_2][\text{Li}(\text{THF})_2]$, the $M_{5,4}$ -edge spectrum is reasonably modeled using a simple Ce^{III} atomic multiplet framework accounting for transitions from a $3d^{10}4f^1$ initial state to a $3d^94f^2$ final state. The 4f–4f Slater–Condon Coulomb repulsion (F_{ff}) and 3d spin–orbit coupling (SOC) parameters were reduced to 60% and 98% of atomic Hartree–Fock values, respectively.¹¹⁷ Reduction of the 4f–4f Slater–Condon Coulomb repulsion (F_{ff}) parameter has been applied in previous studies to account for increased Ce^{3+} bond covalency, and is necessary to accurately model the spectral fine structure. Our previous CI calculations of CeCl_6^{3-} had a F_{ff} reduction to 79% of atomic values, suggesting that the $\text{Ce}(\text{C}_8\text{H}_8)_2^{1-}$ molecule has a higher degree of covalency than CeCl_6^{3-} .

For $\text{Ce}(\text{C}_8\text{H}_8)_2$, a model based on transitions from $3d^{10}4f^0$ to $3d^94f^1$ states does not accurately model the Ce $M_{5,4}$ -edge spectrum, and hence both the initial and final states are described using a charge transfer model. In the charge transfer model, both the initial and final states are defined by two configurations, one of which includes a ligand hole (\underline{L}) resulting from charge transfer. Thus, the initial state is described by $3d^{10}4f^0$ and $3d^{10}\underline{L}4f^1$ and the final state by $3d^94f^1$ and $3d^9\underline{L}4f^1$. These configurations were defined by 4f–4f and 3d–4f Coulomb repulsion, Coulomb exchange and spin–orbit-coupling (SOC) parameters. The interactions of these states were described by the energy separation of the initial (ΔE_{gs}) and final states (ΔE_{fs}) as well as the mixing of each, T_{gs} and T_{fs} respectively. As described previously,⁶⁴ the energy of the lowest LMCT band in the UV/Vis spectrum of $\text{Ce}(\text{C}_8\text{H}_8)_2$ (2.1 eV)⁸ was used to provide bounds for these parameters as governed by $\text{LMCT} \approx \Delta E_{\text{gs}} + 2T_{\text{gs}}$. In addition, the experimentally observed splitting and intensity ratios between the main and satellite peaks in the $M_{5,4}$ -edge XANES spectra provided limits for the calculations. Fig. 5 and Table 2 show that the calculations for $\text{Ce}(\text{C}_8\text{H}_8)_2$ were in the closest agreement with these experimental data were defined with $\Delta E_{\text{gs}} = -0.1$ eV, $\Delta E_{\text{fs}} = -5.0$ eV, and $T_{\text{gs}} = T_{\text{fs}} = 0.75$, resulting in a ground state that was 49% $3d^{10}4f^0$ and 51% $3d^{10}\underline{L}4f^1$, and a calculated LMCT of 2.2 eV. The amount of Ce^{3+} character (51%) calculated for $\text{Ce}(\text{C}_8\text{H}_8)_2$ with CTM4XAS is less than the values determined with L_3 -edge XANES spectroscopy (89%) and multiconfiguration interaction

calculations (80%).^{12,13} Discrepancies with these earlier results, and subtle disagreements with the experimental M-edge spectrum, may reflect the empirical nature of the CTM4XAS calculation. In addition, the CTM4XAS approach cannot shed light on whether the $\text{C} 2p \rightarrow \text{Ce} 4f$ LMCT in $\text{Ce}(\text{C}_8\text{H}_8)_2$ results from simple covalent mixing in the ground state or from coupling of 4f electrons with the ligand π system. However, the results agree qualitatively that the amount $\text{C} 2p \rightarrow \text{Ce} 4f$ LMCT in $\text{Ce}(\text{C}_8\text{H}_8)_2$ exceeds values typically observed for other formal Ce^{4+} compounds such as CeO_2 and CeCl_6^{2-} . In the case of CeCl_6^{2-} , a ground state composition containing 25% of the $3d^{10}\underline{L}4f^1$ configuration was found previously to model the LMCT energy (3.3 eV) as defined by $\Delta E_{\text{gs}} = 2.5$ eV, $\Delta E_{\text{fs}} = -1.5$ eV, and $T_{\text{gs}} = T_{\text{fs}} = 0.70$.⁶⁴ For CeO_2 , the LMCT energy of 3.1 eV was effectively modeled with a ground state containing 30% of the $3d^{10}\underline{L}4f^1$ configuration as defined by $\Delta E_{\text{gs}} = 2.0$ eV, $\Delta E_{\text{fs}} = -1.8$ eV, and $T_{\text{gs}} = T_{\text{fs}} = 0.70$.⁶⁹ Hence, the CTM4XAS calculations and $M_{5,4}$ -edge XAS reveals a trend towards significantly more Ce^{3+} ($3d^{10}\underline{L}4f^1$) character in the ground state of $\text{Ce}(\text{C}_8\text{H}_8)_2$ (51%) than in CeCl_6^{2-} (25%) or CeO_2 (30%).

Carbon K-edge XAS

The background subtracted and normalized C K-edge XAS spectrum of $\text{Ce}(\text{C}_8\text{H}_8)_2$ is shown in Fig. 6 together with previously reported spectra for $\text{Th}(\text{C}_8\text{H}_8)_2$ and $\text{U}(\text{C}_8\text{H}_8)_2$.⁷⁵ Initial evidence for mixing between the Ce 5d and/or 4f orbitals and the C–C π -bonding orbitals of the $[(\text{C}_8\text{H}_8)_2]^{4-}$ ligand framework is provided by existence of pre-edge features at low energy (283 to 287 eV). Analyzing the first derivative of the experimental spectrum (Fig. S1†) revealed two main features centered at 284.2 eV and 286.7 eV that are analogous to features observed at 1–2 eV higher energies in the C K-edge spectra of $\text{Th}(\text{C}_8\text{H}_8)_2$ and

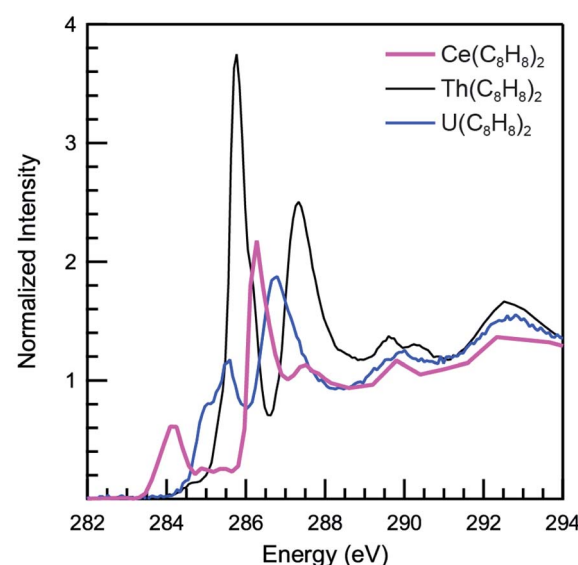


Fig. 6 C K-edge XAS data obtained in transmission for $\text{Ce}(\text{C}_8\text{H}_8)_2$ (pink), $\text{Th}(\text{C}_8\text{H}_8)_2$ (dashed black) and $\text{U}(\text{C}_8\text{H}_8)_2$ (blue). Data for $\text{Th}(\text{C}_8\text{H}_8)_2$ and $\text{U}(\text{C}_8\text{H}_8)_2$ are adapted with permission from ref. 75, copyright 2014 Royal Society of Chemistry.



$\text{U}(\text{C}_8\text{H}_8)_2$.⁷⁵ To a first approximation, the shift to lower energies for $\text{Ce}(\text{C}_8\text{H}_8)_2$ compared to $\text{Th}(\text{C}_8\text{H}_8)_2$ and $\text{U}(\text{C}_8\text{H}_8)_2$ is consistent with expectations based on the lower energy of the Ce 5d and 4f orbitals *versus* 6d and 5f orbitals of Th and U. For additional guidance, energies and oscillator strengths of individual transitions were calculated with TDDFT. Fig. 7 and Table 3 show that the energies calculated by TDDFT correspond well with the experimental data and with the relative energies of orbitals determined from the ground state DFT calculation (Fig. 1). For example, the TDDFT shows a transition from the C 1s orbitals to the antibonding 2e_{2u} (4f- δ) at 284.2 eV, which corresponds to the first low energy feature in the experimental spectrum. At higher energy, the TDDFT shows a second feature at 286.6 eV which includes two overlapping transitions to the antibonding 2e_{3u} (4f- ϕ) orbitals and the nonbonding 1e_{3g} (Ce-C) orbitals, and corresponds to the second feature in the experimental spectrum. The TDDFT calculated difference in energy between the low and high energy feature is 2.4 eV, which is similar to the gap observed experimentally (2.5 eV) and in the ground state DFT calculation (2.96 eV). In addition, transitions with non-negligible oscillator strength involving the 2e_{2g} (5d- δ) orbitals are calculated at 287.9 eV, which agrees well with a weak intensity feature observed in the experimental spectrum at 287.5 eV near the onset of the edge. Transitions to the anti-bonding orbitals of 4f-parentage (2a_{2u} , 2e_{1u} , 1e_{3u}) and 5d-parentage (2a_{1g} , 2e_{1g}) are also observed in the TDDFT calculated spectrum (Table 3), however, the calculated oscillator strengths are small and hence these transitions are unresolved in the experimental spectrum.

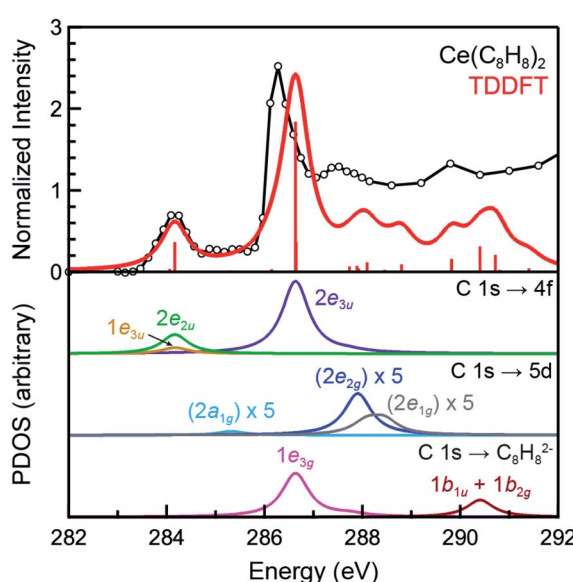


Fig. 7 The experimental C K-edge XAS data for $\text{Ce}(\text{C}_8\text{H}_8)_2$ (black circles and traces) are compared with the TDDFT calculations in the top pane. The red bars represent the energies and oscillator strengths for the individual transitions. The subsequent lower panes depict the partial density of states (PDOS) derived from the TDDFT for final states associated with the 4f, 5d, and ligand-based orbitals. The intensity of the $\text{C} 1\text{s} \rightarrow 5\text{d}$ transitions have been increased by a factor of five for clarity.

Table 3 Comparison of experimental and calculated energies (eV)^a for transitions determined using C K-edge XAS data and TDDFT calculations for $\text{Ce}(\text{C}_8\text{H}_8)_2$

Final state orbital	Transition energies (eV)	
	XAS	TDDFT
$1\text{b}_{1u} + 1\text{b}_{2g}$ (Ce-C nb)	289.0	290.4
2e_{1g} (5d- π)	—	288.3
2e_{2g} (5d- δ)	287.5	287.9
1e_{3g} (Ce-C nb)	286.7	286.6
2e_{3u} (4f- ϕ)	286.7	286.6
2a_{1g} (5d- σ)	285.4	285.3
2e_{1u} (4f- π)	—	284.3
1e_{3u} (4f- ϕ)	284.2	284.2
2e_{2u} (4f- δ)	284.2	284.2
2a_{2u} (4f- σ)	—	284.1

^a Experimental values were determined from a plot of the 1st derivative of the spectrum (Fig. S1). Calculated values were taken from TDDFT simulated spectra and shifted by approximately 10 eV (see Experimental).

Evaluation of $\text{Ce}(\text{C}_8\text{H}_8)_2$ bonding and covalency

The C K-edge pre-edge transition intensities are weighted by the amount of C 2p character, and can be used to evaluate C 2p and Ce 4f mixing in specific molecular orbitals. In some cases, quantifying this effect experimentally was challenged by the presence of overlapping transitions. However, clear patterns in the DFT calculations emerge which are supported by qualitative comparisons of the experimental spectra. For example, the $\text{C} 1\text{s} \rightarrow 2\text{e}_{2g}$ transitions were located at higher energies and unresolved in the experimental spectra; however, the DFT calculations indicate that the composition of the 2e_{2g} (5d- δ) orbitals for $\text{Ce}(\text{C}_8\text{H}_8)_2$ (22% C 2p and 76% Ce 5d) was effectively the same as reported previously for the 2e_{2g} (6d- δ) orbitals of both $\text{Th}(\text{C}_8\text{H}_8)_2$ (23% C 2p and 75% Th 6d) and $\text{U}(\text{C}_8\text{H}_8)_2$ (22% C 2p and 74% U 6d).⁷⁵ Moving to lower energy, transitions attributable to $\text{C} 1\text{s} \rightarrow 1\text{e}_{3u}$ were weak and poorly resolved in the experimental and TDDFT calculated spectrum, and the DFT calculations indicate that the 1e_{3u} (5% C 2p, 95% Ce 4f) and 2e_{3u} (89% C 2p, 7% Ce 4f) are best described as non-bonding metal 4f and ligand-based orbitals, respectively. Similar results were reported previously for $\text{U}(\text{C}_8\text{H}_8)_2$, which had little mixing in the 1e_{3u} (6% C 2p, 94% U 5f) and 2e_{3u} (89% C 2p, 7% U 5f) orbitals. In contrast, evidence for some ϕ -orbital mixing in the unoccupied valence orbitals was observed for $\text{Th}(\text{C}_8\text{H}_8)_2$ as shown by intense pre-edge features associated with the bonding 1e_{3u} (33% C 2p, 65% Th 5f) and antibonding 2e_{3u} (49% C 2p, 47% Th 5f) orbitals.

At low energy, the C K-edge XAS and TDDFT for $\text{Ce}(\text{C}_8\text{H}_8)_2$ show a pre-edge feature at 284.2 eV that was attributed to transitions to the unoccupied δ -antibonding orbitals of 2e_{2u} symmetry, and comparison with the TDDFT spectra suggests that the intensity of this feature reflects a significant contribution of C 2p character. Inspection of the ground state DFT calculations confirms this observation by showing that the 2e_{2u} orbitals have 24% C 2p and 76% Ce 4f character. The 2e_{2u} orbitals are the antibonding counterparts to the bonding 1e_{2u}

orbitals which are occupied in the ground state and have 72% C 2p and 25% Ce 4f character. The DFT calculated mixing of C 2p character into the 4f orbitals is greater than that determined for the analogous 2e_{2u} (5f- δ) orbitals of Th(C₈H₈)₂ (13% C 2p and 86% Th 5f), and only slightly smaller than the mixing of the 2e_{2u} (5f- δ) orbitals for U(C₈H₈)₂ (28% C 2p and 71% U 5f), such that δ -mixing in the 2e_{2u} orbitals increases in the order Th(C₈H₈)₂ < Ce(C₈H₈)₂ \approx U(C₈H₈)₂. Because the 2e_{2u} orbitals are the anti-bonding counterpart to the filled 1e_{2u} orbitals, these results provide new evidence to support earlier theoretical studies^{15,88} that described how the increase in 4f-electron density in Ce(C₈H₈)₂ results from increased δ -mixing with the C₈H₈²⁻ ligands.

However, a more nuanced picture emerges when considering how changes in the radial extension and energy of atomic f-orbitals Ce⁴⁺, Th⁴⁺, and U⁴⁺ affect the nature of covalent bonding with ligand-based orbitals of e_{2u} symmetry. For example, the decrease in 4th ionization energies ($-IE_4/4$)¹¹⁸ from Th (-7.1 eV) to U (-8.3 eV) and results from several theoretical studies^{25,84,92,119-121} suggest that moving from Th⁴⁺ to U⁴⁺ coincides with a decrease in 5f orbital energies. Since the ligand-based orbitals of e_{2u} symmetry are at lower energies, this 5f energy change results in a better energy match (small $E^0(4f) - E^0(\pi_{e_{2u}})$ in eqn (2)) and increased δ -mixing in the 2e_{2u} orbitals for U(C₈H₈)₂. Based on the 4th ionization energy for Ce ($-IE_4/4 = -9.2$ eV),¹²² the 4f orbitals are an even better energy match for the ligand-based e_{2u} orbitals than anticipated for U(C₈H₈)₂. However, the amount of orbital mixing in Ce(C₈H₈)₂ is slightly less than observed for U(C₈H₈)₂. Hence, the very slight difference in covalency for Ce(C₈H₈)₂ relative to U(C₈H₈)₂ is attributed to the decreased radial extension of the 4f orbitals relative to the 5f orbitals¹²³⁻¹²⁶ leading to decreased overlap (smaller H in eqn (2)), which effectively offsets the improved energy match.

The strength of F-orbital bonding

As described above, Ce(C₈H₈)₂ and U(C₈H₈)₂ have qualitatively similar amounts of C 2p mixing with the f-orbitals of e_{2u} symmetry (28% vs. 24% C 2p character, respectively), but different amounts of f-orbital overlap. Consequently, similar amounts of f-orbital mixing does not equate to similar strengths of f-orbital bonding,^{83,127-137} which highlights the counterintuitive relationship between covalency and stability for f-element molecules.¹³⁸ Specifically, the decrease in overlap for Ce(C₈H₈)₂ results in a smaller covalent contribution to the bond energy and more localized electrons. This effect is seen clearly upon examination of splittings between the unoccupied f-orbitals in the ground state (2a_{2u} - 2e_{2u}, Fig. 1 and Table 1), which are significant for U(C₈H₈)₂ (1.23 eV) and small for Ce(C₈H₈)₂ (0.16 eV). In a related study, Cl K-edge XAS and DFT results showed that Cl 3p mixing with the 4f/5f-orbitals was of similar magnitude in CeCl₆²⁻ and UCl₆²⁻ (15.5 and 22.5% Cl 3p character per bond, respectively) although the two compounds have very different ligand field splitting parameters (θ , t_{1u} - t_{2u}: 0.01 vs. 0.22 eV, respectively).^{62,64,139,140} The ground state electron density calculations of Kerridge also support this interpretation, showing

that the f-electrons are more delocalized for U(C₈H₈)₂ than for Ce(C₈H₈)₂ or transuranic actinocenes.^{17,49}

The question of whether f-orbital covalency confers stability to Ce(C₈H₈)₂, Th(C₈H₈)₂, and U(C₈H₈)₂ has also been considered during analyses of their varying physical characteristics and chemical reactivities. For example, the fact that U(C₈H₈)₂ has a low sublimation point, while Th(C₈H₈)₂ and Ce(C₈H₈)₂ do not sublime easily without decomposition, has been partially attributed to the greater strength of 5f orbital bonding in U(C₈H₈)₂.^{9,141} Following early reports which showed that U(C₈H₈)₂ hydrolyzes slowly at room temperature while Ce(C₈H₈)₂ and Th(C₈H₈)₂ hydrolyze instantaneously,¹ Moore and Streitwieser performed a quantitative analysis of hydrolysis reactions for a range of M₂(C₈H₈) and M(C₈H₈)₂ compounds (M = Li, K, Cs and Ce, Th, U).¹⁴² In summary, it was hypothesized that under equilibrium conditions slower hydrolysis would result in greater formation of the more conjugated 1,3,5-cyclooctatriene isomer (thermodynamic product) relative to the 1,3,6-cyclooctatriene isomer (kinetic product).¹⁴³ The opposite effect was observed, such that significant increases in the amount of 1,3,6-C₈H₁₀ were observed when varying the metal from Cs to K to Li or from Ce to Th to U (Table 4). Competition experiments with D₂O suggested that, for U(C₈H₈)₂ and Li₂(C₈H₈), the rate of protonation of the C₈H₈²⁻ ligands *via* uncomplexed water molecules slowed, and prior coordination to the metal cation by the water molecule before protonation became competitive. The resultant change in the regiochemistry of protonation explained why U(C₈H₈)₂ and Li₂(C₈H₈) formed more of the 1,3,6-C₈H₁₀ isomer, while using other M(C₈H₈)₂ and M(C₈H₈) complexes or more acidic proton sources increased the relative amount of 1,3,5-C₈H₁₀ formation.

Taken together with the spectroscopic and theory results presented above, the work of Moore and Streitwieser suggests that practical hypotheses pertaining to the chemical reactivities of the lanthanides, thorium, uranium, and transuranic actinides can be derived by accounting for differences in d- and f-orbital overlap.¹⁴⁴⁻¹⁵¹ With the exception of Li₂(C₈H₈),

Table 4 Reactivity data reported previously by Moore,¹⁴² showing the ratio of cyclooctatriene (C₈H₁₀) isomers formed following hydrolysis of C₈H₈²⁻ complexes in a degassed, 1 M solution of H₂O in THF. The isomers were separated using gas chromatography and analyzed by ¹H NMR to determine the ratio. The thermodynamic equilibrium ratio of C₈H₁₀ isomers is 40 : 1, 1,3,5-C₈H₁₀ to 1,3,6-C₈H₁₀.¹⁴³

Starting material	Cyclooctatriene isomer ^a (%)	
	1,3,5-C ₈ H ₁₀	1,3,6-C ₈ H ₁₀
M₂(C₈H₈) complexes		
Li ₂ (C ₈ H ₈)	43	57
K ₂ (C ₈ H ₈)	76	24
Cs ₂ (C ₈ H ₈)	79	21
M(C₈H₈)₂ complexes		
Ce(C ₈ H ₈) ₂	62	38
Th(C ₈ H ₈) ₂	49	51
U(C ₈ H ₈) ₂	36	64

^a Reported confidence in the percentages was 2%.¹⁴²



formation of the 1,3,6-C₈H₁₀ isomer was decreased for all M₂(C₈H₈) relative to M(C₈H₈)₂, which may reflect stabilization of M(C₈H₈)₂ complexes due to mixing with the diffuse 5d- and 6d-orbitals. Similarly, 5f orbital participation in bonding confers stability to U(C₈H₈)₂ because there is a degree of overlap between the U 5f orbitals. Without a similar degree of overlap, 4f-orbital mixing in Ce(C₈H₈)₂ is accompanied by an overall weakening of the complex due to a comparatively large drop in the strength of ionic bonding.^{62,83,84,127–129}

Conclusion

In consideration of the large body of experimental and theoretical work reported previously and cited above, the C K-edge results described herein provide the first direct experimental evidence for covalent mixing between the Ce 4f/5d and the ligand-based C 2p orbitals in Ce(C₈H₈)₂. Ce 5d mixing in Ce(C₈H₈)₂ was greatest for the δ -symmetry e_{2g} orbitals, and ground-state DFT calculations show comparable mixing in the 6d-orbitals of e_{2g} symmetry for both Th(C₈H₈)₂ and U(C₈H₈)₂. The Ce M_{5,4}-edge XAS and CI calculations provide evidence for Ce 4f mixing by showing that contributions of the 4f¹L³ configuration (Ce³⁺) to the ground state of Ce(C₈H₈)₂ are similar to intermetallic compounds such as CeRh₃ and significantly larger than observed for other formally Ce⁴⁺ compounds including CeO₂ and CeCl₆²⁻. The ground-state DFT and TDDFT study shows that Ce 4f and C 2p orbital mixing occurs largely in the δ -bonding orbitals of e_{2u} symmetry, and comparisons with earlier DFT and C K-edge studies show that the magnitude of e_{2u} mixing is similar for Ce(C₈H₈)₂ and U(C₈H₈)₂. A simple theoretical framework was provided to rationalize these results, in which covalency in U(C₈H₈)₂ is partially the result of productive overlap between the C 2p and relatively diffuse 5f orbitals. In contrast, metal-ligand overlap decreases with the more contracted 4f orbitals of Ce(C₈H₈)₂, but this is effectively offset by the smaller metal-ligand energy mismatch obtained with the lower energy 4f orbitals. Although covalent orbital mixing was similar for Ce(C₈H₈)₂ and U(C₈H₈)₂, the differences in orbital overlap resulted in a greater covalent contribution to stability for U(C₈H₈)₂ and greater reactivity for Ce(C₈H₈)₂. Taken together, these results show how – in the absence of significant orbital overlap – increases in orbital mixing allow the 4f-electrons in Ce(C₈H₈)₂ to participate in bonding while appearing localized simultaneously. We are currently extending these analyses to the transuranic analogues (C₈H₈)₂An (An = Np, Pu, Am, Cm) to further our understanding of how bonding and electronic structure varies across the f-block elements.

Experimental

STXM sample preparation

All manipulations were performed with rigorous exclusion of air and moisture using Schlenk and glovebox techniques under an argon atmosphere. Toluene (Fisher) was distilled from sodium metal and benzophenone prior to use. Ce(C₈H₈)₂ and [Li(THF)]₂[Ce(C₈H₈)₂] were prepared using the literature procedure.⁹ To prepare each sample, a small amount (\sim 1 mg) was dissolved in

toluene (1 mL), and an aliquot of the solution (0.5 μ L) was transferred to a Si₃N₄ window (100 nm, Silson) using a micro-pipette. The toluene was allowed to evaporate over a few seconds, which deposited thin crystallites of the sample on the Si₃N₄ membrane. After drying for several more minutes, a second window was placed over the sample, sandwiching the crystallites, and the windows were sealed together using Hardman Double/Bubble® epoxy.

STXM-XAS measurements and data analysis

The STXM methodology was similar to that discussed previously.^{64,75,76} Single-energy images and XAS data were acquired using the STXM instruments at the Advanced Light Source-Molecular Environmental Science (ALS-MES) beamline 11.0.2 and at the Canadian Light Source (CLS) spectromicroscopy beamline 10ID-1. The ALS operated in topoff mode (500 mA) and the CLS operated in decay mode (250 to 150 mA). At both facilities, the beamlines operated with \sim 0.5 atm He-filled chambers and used elliptically polarizing undulators that delivered photons to entrance slit-less plane-grating monochromators.¹⁰³ An energy calibration was performed at the C K-edge for CO₂ gas (294.95 eV) and at the Ne K-edge for Ne gas (867.30 eV). For these measurements, the X-ray beam was focused with a zone plate onto the sample, and the transmitted photons were detected as function of the energy and sample position. The spot size and spatial resolution were determined from characteristics of the 35 nm zone plate. The energy resolution was estimated at 0.04 eV at the C K-edge and 0.10 at the Ce M-edges, and spectra were collected using circularly polarized radiation to obviate polarization effects. To minimize the impact of radiation damage during spectral acquisitions, individual C K-edge and Ce M₅-edge scan times were reduced by limiting the scan range to 50–60 total energy points (130 energy points for full Ce M_{5,4}-edge data), by setting the dwell time to 1 ms per pixel, and by reducing the number of pixels over a target area such that no less than 0.01 μ m² per pixel was achieved. Radiation damage was characterized as shown in Fig. 3 by repeating these scans on the same target area. Spectra that were most representative of undamaged Ce(C₈H₈)₂ were acquired by averaging individual scans obtained from multiple target areas. The C K-edge data were normalized in MATLAB using the MBACK algorithm,¹⁵² and by setting the edge jump at 295 eV to an intensity of 1.0. For Ce M_{5,4}-edge data, a line was fit to the pre-edge region below 875 eV and then subtracted from the experimental data to eliminate the background of the spectrum. First-derivative spectra were used as guides to determine the number and position of peaks (see ESI, Fig. S1–S3†).

Electronic structure calculations

Ground state electronic structure calculations were performed on Ce(C₈H₈)₂ using B3LYP hybrid DFT,^{153,154} in the Gaussian 09 code.¹⁵⁵ Ce was modeled with the Stuttgart relativistic effective core potential (ecp) and basis set^{156–158} while C and H were modeled using a Pople style double- ζ 6–31 G(d',p') basis set with polarization functions optimized for heavy atoms.¹⁵⁹ These functionals and basis sets have demonstrated good agreement between experimental and simulated ligand K-edge



XAS spectra for organometallic and inorganic systems.^{62,75} The molecular orbital composition of $\text{Ce}(\text{C}_8\text{H}_8)_2$ was obtained by Mulliken population analysis of the individual molecular orbitals.

CI calculations

Multiplet calculations were implemented using CTM4XAS, which is a program based on the original code by Cowan¹¹² and further developed by de Groot.^{113,114} Effects of the crystal field are typically minimal in f-systems, so they were not included,¹¹² and a detailed summary of this method was previously described.⁶⁴ The $[(\text{COT})_2\text{Ce}]^{1-}$ configurations were defined by 4f-4f Coulomb repulsion (F_{ff}) reduced to 60% of atomic values, Coulomb 3d-4f repulsion (F_{fd}) at atomic values, 3d-4f Coulomb exchange (G_{fd}) at atomic values, and SOC reduced to 98% of atomic values. A Gaussian broadening of 0.25 eV was applied to account for instrumental broadening and Lorentzian broadenings of 0.2 and 0.5 eV were applied to the M_5 and M_4 edges, respectively. The $(\text{COT})_2\text{Ce}$ configurations were defined by 4f-4f Coulomb repulsion (F_{ff}) at atomic values, Coulomb 3d-4f repulsion (F_{fd}) reduced to 63% of atomic values, 3d-4f Coulomb exchange (G_{fd}) reduced to 90% of atomic values, and SOC reduced to 96% of atomic values. For the $3\text{d}^94\text{f}^1$ configuration this resulted in values of $F_{\text{fd}} = 4.130$, $G_{\text{fd}} = 4.074$, and SOC = 7.144 eV. For the $3\text{d}^9\text{L}4\text{f}^2$ configuration this resulted in values of $F_{\text{fd}} = 3.774$, $G_{\text{fd}} = 3.653$, and SOC = 7.148 eV. Additionally, the parameter space was defined by $\Delta E_{\text{gs}} = -0.1$ eV, $\Delta E_{\text{fs}} = -5.0$ eV, and $T_{\text{gs}} = T_{\text{fs}} = 0.75$. A Gaussian broadening of 0.35 eV was applied to account for instrumental broadening and Lorentzian broadenings of 0.3 and 0.6 eV were applied to the M_5 and M_4 edges, respectively.

Simulated C K-Edge spectra

For $\text{Ce}(\text{C}_8\text{H}_8)_2$, the C K-edge XAS spectra was simulated using TDDFT as described previously.^{75,76} An energy shift was established to account for the omission of the atomic relaxation associated with the core excitation, relativistic stabilization, and errors associated with the functional. This was achieved by setting the energy of transitions simulated for the antibonding 2e_{2u} (5f- δ) orbitals to be equal to those in the experimental spectra, which resulted in an energy shift of +9.93 eV.

Author contributions

Clark, Kozimor, and Shuh oversaw the spectroscopic research, and Minasian conceived of the experiments. Minasian, Shuh and Tyliszczak performed the experiments, and Minasian and Smiles analyzed the data. Batista, Keith, and Martin performed the DFT calculations, and Stieber performed CI calculations. All authors participated in writing the manuscript.

Conflicts of interest

There are no conflicts to declare.

Acknowledgements

We thank Professor Richard Andersen for providing the sample of $\text{Ce}(\text{C}_8\text{H}_8)_2$. This research was supported equally by the Director, Office of Science, Office of Basic Energy Sciences, Division of Chemical Sciences, Geosciences, and Biosciences (CSGB), Heavy Element Chemistry program of the U.S. Department of Energy (DOE) under contract no. DE-AC02-05CH11231 at LBNL (Booth, Minasian, Shuh, Smiles) and by the Director, Office of Science, Office of Basic Energy Sciences, Division of CSGB, Heavy Element Chemistry program of the U.S. DOE at LANL (Batista, Clark, Keith, Kozimor, Martin). Los Alamos National Laboratory is operated by Los Alamos National Security, LLC, for the National Nuclear Security Administration of U.S. Department of Energy (contract no. DE-AC52-06NA25396). Stieber acknowledges CPP College of Science, a CSUPERB New Investigator Grant, and NSF XSEDE (CHE160059). STXM research described in this paper was conducted at the Canadian Light Source, which is supported by the Canada Foundation for Innovation, Natural Sciences and Engineering Research Council of Canada, the University of Saskatchewan, the Government of Saskatchewan, Western Economic Diversification Canada, the National Research Council Canada, and the Canadian Institutes of Health Research. Additional STXM research done at ALS beamline 11.0.2 and Tyliszczak were supported by the Director of the Office of Science, Office of Basic Energy Sciences, of the U.S. Department of Energy under Contract No. DE-AC02-05CH11231.

References

- 1 A. Greco, S. Cesca and G. Bertolini, *J. Organomet. Chem.*, 1976, **113**, 321–330.
- 2 A. Streitwieser, S. A. Kinsley, J. T. Rigsbee, I. L. Fragala, E. Ciliberto and N. Rösch, *J. Am. Chem. Soc.*, 1985, **107**, 7786–7788.
- 3 K. N. Raymond and C. W. Eigenbrot, *Acc. Chem. Res.*, 1980, **13**, 276–283.
- 4 U. Kilimann, R. Herbst-Irmer, D. Stalke and F. T. Edelmann, *Angew. Chem., Int. Ed.*, 1994, **33**, 1618–1621.
- 5 T. R. Boussie, D. C. Eisenberg, J. Rigsbee, A. Streitwieser and A. Zalkin, *Organometallics*, 1991, **10**, 1922–1928.
- 6 V. Lorenz, B. M. Schmiege, C. G. Hrib, J. W. Ziller, A. Edelmann, S. Blaurock, W. J. Evans and F. T. Edelmann, *J. Am. Chem. Soc.*, 2011, **133**, 1257–1259.
- 7 K. O. Hodgson and K. N. Raymond, *Inorg. Chem.*, 1972, **11**, 3030–3035.
- 8 A. Streitwieser, S. A. Kinsley, C. H. Jenson and J. T. Rigsbee, *Organometallics*, 2004, **23**, 5169–5175.
- 9 M. D. Walter, C. H. Booth, W. W. Lukens and R. A. Andersen, *Organometallics*, 2009, **28**, 698–707.
- 10 J. P. Clark and J. C. Green, *J. Chem. Soc., Dalton Trans.*, 1977, 505–508.
- 11 J. G. Brennan, J. C. Green and C. M. Redfern, *J. Am. Chem. Soc.*, 1989, **111**, 2373–2377.
- 12 M. Dolg, P. Fulde, H. Stoll, H. Preuss, A. Chang and R. M. Pitzer, *Chem. Phys.*, 1995, **195**, 71–82.



13 M. Dolg, P. Fulde, W. Küchle, C.-S. Neumann and H. Stoll, *J. Chem. Phys.*, 1991, **94**, 3011–3017.

14 W. J. Liu, M. Dolg and P. Fulde, *J. Chem. Phys.*, 1997, **107**, 3584–3591.

15 A. Kerridge, R. Coates and N. Kaltsoyannis, *J. Phys. Chem. A*, 2009, **113**, 2896–2905.

16 O. Mooßen and M. Dolg, *Chem. Phys. Lett.*, 2014, **594**, 47–50.

17 A. Kerridge, *Dalton Trans.*, 2013, **42**, 16428–16436.

18 N. M. Edelstein, P. G. Allen, J. J. Bucher, D. K. Shuh, C. D. Sofield, N. Kaltsoyannis, G. H. Maunder, M. R. Russo and A. Sella, *J. Am. Chem. Soc.*, 1996, **118**, 13115–13116.

19 H.-D. Amberger, H. Reddmann and F. T. Edelmann, *J. Organomet. Chem.*, 2005, **690**, 2238–2242.

20 C. H. Booth, M. D. Walter, M. Daniel, W. W. Lukens and R. A. Andersen, *Phys. Rev. Lett.*, 2005, **95**, 267202.

21 G. Kaindl, G. Schmiester, E. V. Sampathkumaran and P. Wachter, *Phys. Rev. B: Condens. Matter Mater. Phys.*, 1988, **38**, 10174–10177.

22 T. K. Sham, R. A. Gordon and S. M. Heald, *Phys. Rev. B: Condens. Matter Mater. Phys.*, 2005, **72**, 035113.

23 A. Kotani, *Mod. Phys. Lett. B*, 2013, **27**, 1330012.

24 J. J. Kas, J. J. Rehr and J. B. Curtis, *Phys. Rev. B*, 2016, 94.

25 M. L. Neidig, D. L. Clark and R. L. Martin, *Coord. Chem. Rev.*, 2013, **257**, 394–406.

26 A. Kotani, K. O. Kvashnina, S. M. Butorin and P. Glatzel, *Eur. Phys. J. B*, 2012, **85**, 257.

27 A. Ashley, G. Balazs, A. Cowley, J. Green, C. H. Booth and D. O'Hare, *Chem. Commun.*, 2007, 1515–1517.

28 M. Coreno, M. de Simone, J. C. Green, N. Kaltsoyannis, N. Narband and A. Sella, *Chem. Phys. Lett.*, 2006, **432**, 17–21.

29 A. Kerridge and N. Kaltsoyannis, *C. R. Chim.*, 2010, **13**, 853–859.

30 G. Balazs, F. G. N. Cloke, J. C. Green, R. M. Harker, A. Harrison, P. B. Hitchcock, C. N. Jardine and R. Walton, *Organometallics*, 2007, **26**, 3111–3119.

31 D. Werner, G. B. Deacon, P. C. Junk and R. Anwander, *Dalton Trans.*, 2017, **46**, 6265–6277.

32 L. A. Solola, A. V. Zabula, W. L. Dorfner, B. C. Manor, P. J. Carroll and E. J. Schelter, *J. Am. Chem. Soc.*, 2016, **138**, 6928–6931.

33 L. A. Solola, A. V. Zabula, W. L. Dorfner, B. C. Manor, P. J. Carroll and E. J. Schelter, *J. Am. Chem. Soc.*, 2017, **139**, 2435–2442.

34 I. J. Casely, S. T. Liddle, A. J. Blake, C. Wilson and P. L. Arnold, *Chem. Commun.*, 2007, 5037–5039.

35 Y. M. So, Y. Li, K. C. Au-Yeung, G. C. Wang, K. L. Wong, H. H. Y. Sung, P. L. Arnold, I. D. Williams, Z. Y. Lin and W. H. Leung, *Inorg. Chem.*, 2016, **55**, 10003–10012.

36 L. Eyring, in *Synthesis of Lanthanide and Actinide Compounds*, ed. G. Meyer and L. R. Morss, Springer Science, Dordrecht, 1991.

37 B. G. Müller, in *Synthesis of Lanthanide and Actinide Compounds*, ed. G. Meyer and L. R. Morss, Springer Science, Dordrecht, 1991.

38 Q. N. Zhang, S. X. Hu, H. Qu, J. Su, G. J. Wang, J. B. Lu, M. H. Chen, M. F. Zhou and J. Li, *Angew. Chem., Int. Ed.*, 2016, **55**, 6896–6900.

39 A. Kovacs, P. D. Dau, J. Marcalo and J. K. Gibson, *Inorg. Chem.*, 2018, **57**, 9453–9467.

40 N. T. Rice, I. A. Popov, D. R. Russo, J. Bacsa, E. R. Batista, P. Yang, J. Telser and H. S. La Pierre, *J. Am. Chem. Soc.*, 2019, **141**, 13222–13233.

41 C. T. Palumbo, I. Zivkovic, R. Scopelliti and M. Mazzanti, *J. Am. Chem. Soc.*, 2019, **141**, 9827–9831.

42 G. Nocton, W. W. Lukens, C. H. Booth, S. S. Rozenel, S. A. Medling, L. Maron and R. A. Andersen, *J. Am. Chem. Soc.*, 2014, **136**, 8626–8641.

43 G. Nocton, C. H. Booth, L. Maron and R. A. Andersen, *Organometallics*, 2013, **32**, 5305–5312.

44 C. H. Booth, M. D. Walter, D. Kazhdan, Y. J. Hu, W. W. Lukens, E. D. Bauer, L. Maron, O. Eisenstein and R. A. Andersen, *J. Am. Chem. Soc.*, 2009, **131**, 6480–6491.

45 C. H. Booth, D. Kazhdan, E. L. Werkema, M. D. Walter, W. W. Lukens, E. D. Bauer, Y. J. Hu, L. Maron, O. Eisenstein, M. Head-Gordon and R. A. Andersen, *J. Am. Chem. Soc.*, 2010, **132**, 17537–17549.

46 M. Coreno, M. de Simone, R. Coates, M. S. Denning, R. G. Denning, J. C. Green, C. Hunston, N. Kaltsoyannis and A. Sella, *Organometallics*, 2010, **29**, 4752–4755.

47 R. G. Denning, J. Harmer, J. C. Green and M. Irwin, *J. Am. Chem. Soc.*, 2011, **133**, 20644–20660.

48 W. W. Lukens, N. Magnani and C. H. Booth, *Inorg. Chem.*, 2012, **51**, 10105–10110.

49 A. Kerridge, *RSC Adv.*, 2014, **4**, 12078–12086.

50 S.-X. Hu, W.-L. Li, J.-B. Lu, J. L. Bao, H. S. Yu, D. G. Truhlar, J. K. Gibson, J. Marcalo, M. Zhou, S. Riedel, W. H. E. Schwarz and J. Li, *Angew. Chem., Int. Ed.*, 2018, **57**, 3242–3245.

51 P. T. Wolczanski, *Organometallics*, 2017, **36**, 622–631.

52 G. R. Choppin, *J. Alloys Compd.*, 2002, **344**, 55–59.

53 W. J. Liang, M. P. Shores, M. Bockrath, J. R. Long and H. Park, *Nature*, 2002, **417**, 725–729.

54 J. Park, A. N. Pasupathy, J. I. Goldsmith, C. Chang, Y. Yaish, J. R. Petta, M. Rinkoski, J. P. Sethna, H. D. Abruna, P. L. McEuen and D. C. Ralph, *Nature*, 2002, **417**, 722–725.

55 S. Demir, M. Nippe, M. I. Gonzalez and J. R. Long, *Chem. Sci.*, 2014, **5**, 4701–4711.

56 K. L. M. Harriman, J. L. Brosmer, L. Ungur, P. L. Diaconescu and M. Murugesu, *J. Am. Chem. Soc.*, 2017, **139**, 1420–1423.

57 L. Ungur, J. J. Le Roy, I. Korobkov, M. Murugesu and L. F. Chibotaru, *Angew. Chem., Int. Ed.*, 2014, **53**, 4413–4417.

58 X.-W. Chi, Q.-Y. Wu, J.-H. Lan, C.-Z. Wang, Q. Zhang, Z.-F. Chai and W.-Q. Shi, *Organometallics*, 2019, **38**, 1963–1972.

59 C. P. Burns, X. Yang, S. Y. Sung, J. D. Wofford, N. S. Bhuvanesh, M. B. Hall and M. Nippe, *Chem. Commun.*, 2018, **54**, 10893–10896.

60 T. P. Latendresse, V. Vieru, B. O. Wilkins, N. S. Bhuvanesh, L. F. Chibotaru and M. Nippe, *Angew. Chem., Int. Ed.*, 2018, **57**, 8164–8169.



61 J. N. Cross, J. Su, E. R. Batista, S. K. Cary, W. J. Evans, S. A. Kozimor, V. Mocko, B. L. Scott, B. W. Stein, C. J. Windorff and P. Yang, *J. Am. Chem. Soc.*, 2017, **139**, 8667–8677.

62 S. G. Minasian, J. M. Keith, E. R. Batista, K. S. Boland, C. N. Christensen, D. L. Clark, S. D. Conradson, S. A. Kozimor, R. L. Martin, D. E. Schwarz, D. K. Shuh, G. L. Wagner, M. P. Wilkerson, L. E. Wolfsberg and P. Yang, *J. Am. Chem. Soc.*, 2012, **134**, 5586–5597.

63 S. R. Daly, J. M. Keith, E. R. Batista, K. S. Boland, D. L. Clark, S. A. Kozimor and R. L. Martin, *J. Am. Chem. Soc.*, 2012, **134**, 14408–14422.

64 M. W. Löble, J. M. Keith, A. B. Altman, S. C. E. Stieber, E. R. Batista, K. S. Boland, S. D. Conradson, D. L. Clark, J. Lezama Pacheco, S. A. Kozimor, R. L. Martin, S. G. Minasian, A. C. Olson, B. L. Scott, D. K. Shuh, T. Tyliszczak, M. P. Wilkerson and R. A. Zehnder, *J. Am. Chem. Soc.*, 2015, **137**, 2506–2523.

65 S. E. Shadle, B. Hedman, K. O. Hodgson and E. I. Solomon, *Inorg. Chem.*, 1994, **33**, 4235–4244.

66 S. E. Shadle, B. Hedman, K. O. Hodgson and E. I. Solomon, *J. Am. Chem. Soc.*, 1995, **117**, 2259–2272.

67 S. D. George, P. Brant and E. I. Solomon, *J. Am. Chem. Soc.*, 2005, **127**, 667–674.

68 E. I. Solomon, B. Hedman, K. O. Hodgson, A. Dey and R. K. Szilagyi, *Coord. Chem. Rev.*, 2005, **249**, 97–129.

69 S. G. Minasian, E. R. Batista, C. H. Booth, D. L. Clark, J. M. Keith, S. A. Kozimor, W. W. Lukens, R. L. Martin, D. K. Shuh, S. C. E. Stieber, T. Tyliszczak and X. D. Wen, *J. Am. Chem. Soc.*, 2017, **139**, 18052–18064.

70 A. B. Altman, J. I. Pacold, J. Wang, W. W. Lukens and S. G. Minasian, *Dalton Trans.*, 2016, **45**, 9948–9961.

71 S. G. Minasian, J. M. Keith, E. R. Batista, K. S. Boland, J. A. Bradley, S. R. Daly, S. A. Kozimor, W. W. Lukens, R. L. Martin, D. Nordlund, G. T. Seidler, D. K. Shuh, D. Sokaras, T. Tyliszczak, G. L. Wagner, T.-C. Weng and P. Yang, *J. Am. Chem. Soc.*, 2013, **135**, 1864–1871.

72 J. T. Lukens, I. M. DiMucci, T. Kurogi, D. J. Mindiola and K. M. Lancaster, *Chem. Sci.*, 2019, **10**, 5044–5055.

73 T. Dumas, D. Guillaumont, C. Filliaux, A. Scheinost, P. Moisy, S. Petit, D. K. Shuh, T. Tyliszczak and C. Den Auwer, *Phys. Chem. Chem. Phys.*, 2016, **18**, 2887–2895.

74 C. D. Pemmaraju, R. Copping, S. Wang, M. Janousch, S. J. Teat, T. Tyliszczak, A. Canning, D. K. Shuh and D. Prendergast, *Inorg. Chem.*, 2014, **53**, 11415–11425.

75 S. G. Minasian, J. M. Keith, E. R. Batista, K. S. Boland, D. L. Clark, S. A. Kozimor, R. L. Martin, D. K. Shuh and T. Tyliszczak, *Chem. Sci.*, 2014, **5**, 351–359.

76 S. G. Minasian, J. M. Keith, E. R. Batista, K. S. Boland, S. A. Kozimor, R. L. Martin, D. K. Shuh, T. Tyliszczak and L. J. Vernon, *J. Am. Chem. Soc.*, 2013, **135**, 14731–14740.

77 J. C. Green, *Struct. Bonding*, 1981, **43**, 37–112.

78 A. Streitwieser and C. A. Harmon, *Inorg. Chem.*, 1973, **12**, 1102–1104.

79 J. Li and B. E. Bursten, *J. Am. Chem. Soc.*, 1998, **120**, 11456–11466.

80 A. H. H. Chang and R. M. Pitzer, *J. Am. Chem. Soc.*, 1989, **111**, 2500–2507.

81 K. D. Warren, *Struct. Bonding*, 1977, **33**, 97–138.

82 J. A. Platts and R. J. Baker, *Dalton Trans.*, 2020, **49**, 1077–1088.

83 T. A. Pham, A. B. Altman, S. C. E. Stieber, C. H. Booth, S. A. Kozimor, W. W. Lukens, D. T. Olive, T. Tyliszczak, J. Wang, S. G. Minasian and K. N. Raymond, *Inorg. Chem.*, 2016, **55**, 9989–10002.

84 N. Kaltsoyannis, *Inorg. Chem.*, 2013, **52**, 3407–3413.

85 C. J. Cramer, *Essentials of Computational Chemistry*, Wiley, Chichester, UK, 2nd edn, 2004.

86 S. A. Kozimor, P. Yang, E. R. Batista, K. S. Boland, C. J. Burns, C. N. Christensen, D. L. Clark, S. D. Conradson, P. J. Hay, J. S. Lezama, R. L. Martin, D. E. Schwarz, M. P. Wilkerson and L. E. Wolfsberg, *Inorg. Chem.*, 2008, **47**, 5365–5371.

87 A. C. Olson, J. M. Keith, E. R. Batista, K. S. Boland, S. R. Daly, S. A. Kozimor, M. M. MacInnes, R. L. Martin and B. L. Scott, *Dalton Trans.*, 2014, **43**, 17283–17295.

88 N. Rösch, *Inorg. Chim. Acta*, 1984, **94**, 297–299.

89 F. Ferraro, C. A. Barboza and R. Arratia-Pérez, *J. Phys. Chem. A*, 2012, **116**, 4170–4175.

90 E. Solis-Cespedes and D. Paez-Hernandez, *Dalton Trans.*, 2017, **46**, 4834–4843.

91 P. M. Boerrigter, E. J. Baerends and J. G. Snijders, *Chem. Phys.*, 1988, **122**, 357–374.

92 M. Pepper and B. E. Bursten, *Chem. Rev.*, 1991, **91**, 719–741.

93 M. Koga, W. J. Liu, M. Dolg and P. Fulde, *Phys. Rev. B: Condens. Matter Mater. Phys.*, 1998, **57**, 10648–10654.

94 A. Kerridge and N. Kaltsoyannis, *J. Phys. Chem. A*, 2009, **113**, 8737–8745.

95 F. M. F. de Groot, *Coord. Chem. Rev.*, 2005, **249**, 31–63.

96 B. Vlaisayljevich, P. L. Diaconescu, W. L. Lukens, L. Gagliardi and C. C. Cummins, *Organometallics*, 2013, **32**, 1341–1352.

97 C. S. Neumann and P. Fulde, *Z. Phys. B: Condens. Matter*, 1989, **74**, 277–278.

98 P. S. Riseborough, *Adv. Phys.*, 2000, **49**, 257–320.

99 G. Anne, N. S. Vidhyadhiraja and E. L. David, *J. Phys.: Condens. Matter*, 2007, **19**, 106220.

100 L. Gagliardi, *Int. J. Quantum Chem.*, 2011, **111**, 3302–3306.

101 J. L. Jung, M. Atanasov and F. Neese, *Inorg. Chem.*, 2017, **56**, 8802–8816.

102 E. R. Batista and R. L. Martin, *J. Am. Chem. Soc.*, 2007, **129**, 7224–7225.

103 H. Bluhm, K. Andersson, T. Araki, K. Benzerara, G. E. Brown, J. J. Dynes, S. Ghosal, M. K. Gilles, H. C. Hansen, J. C. Hemminger, A. P. Hitchcock, G. Ketteler, A. L. D. Kilcoyne, E. Kneedler, J. R. Lawrence, G. G. Leppard, J. Majzlam, B. S. Mun, S. C. B. Myneni, A. Nilsson, H. Ogasawara, D. F. Ogletree, K. Pecher, M. Salmeron, D. K. Shuh, B. Tonner, T. Tyliszczak, T. Warwick and T. H. Yoon, *J. Electron Spectrosc. Relat. Phenom.*, 2006, **150**, 86–104.

104 S. Hanhan, A. M. Smith, M. Obst and A. P. Hitchcock, *J. Electron Spectrosc. Relat. Phenom.*, 2009, **173**, 44–49.



105 G. Kaindl, G. Kalkowski, W. D. Brewer, E. V. Sampathkumaran, F. Holtzberg and A. S. Vonwittenau, *J. Magn. Magn. Mater.*, 1985, **47–8**, 181–189.

106 T. Jo and A. Kotani, *J. Phys. Soc. Jpn.*, 1988, **57**, 2288–2291.

107 G. Kaindl, G. Kalkowski, W. D. Brewer, B. Perscheid and F. Holtzberg, *J. Appl. Phys.*, 1984, **55**, 1910–1915.

108 B. T. Thole, G. Vanderlaan, J. C. Fuggle, G. A. Sawatzky, R. C. Karnatak and J. M. Esteva, *Phys. Rev. B*, 1985, **32**, 5107–5118.

109 A. Kotani and H. Ogasawara, *J. Electron Spectrosc. Relat. Phenom.*, 1992, **60**, 257–299.

110 P. Le Fevre, H. Magnan, J. Vogel, V. Formoso, K. Hricovini and D. Chandesris, *J. Synchrotron Radiat.*, 1999, **6**, 290–292.

111 H. Ogasawara, A. Kotani, P. Le Fevre, D. Chandesris and H. Magnan, *Phys. Rev. B: Condens. Matter Mater. Phys.*, 2000, **62**, 7970–7975.

112 R. D. Cowan, *Theory of Atomic Structure and Spectra*, University of California Press, 1981.

113 F. M. F. de Groot and A. Kotani, *Core Level Spectroscopy of Solids*, Taylor and Francis, New York, 2008.

114 E. Stavitski and F. M. F. de Groot, *Micron*, 2010, **41**, 687–694.

115 S. O. Kucheyev, B. J. Clapsaddle, Y. M. Wang, T. van Buuren and A. V. Hamza, *Phys. Rev. B: Condens. Matter Mater. Phys.*, 2007, **76**, 235420.

116 S. Turner, S. Lazar, B. Freitag, R. Egoavil, J. Verbeeck, S. Put, Y. Strauven and G. Van Tendeloo, *Nanoscale*, 2011, **3**, 3385–3390.

117 K. O. Hodgson, F. Mares, D. F. Starks and A. Streitwieser, *J. Am. Chem. Soc.*, 1973, **95**, 8650–8658.

118 X. Y. Cao and M. Dolg, *J. Mol. Struct.*, 2004, **673**, 203–209.

119 I. D. Prodan, G. E. Scuseria and R. L. Martin, *Phys. Rev. B: Condens. Matter Mater. Phys.*, 2007, **76**, 033101.

120 M. J. Tassell and N. Kaltsoyannis, *Dalton Trans.*, 2010, **39**, 6719–6725.

121 I. Kirker and N. Kaltsoyannis, *Dalton Trans.*, 2011, **40**, 124–131.

122 W. C. Martin, R. Zalubas and L. Hagan, *Atomic Energy Levels – The Rare Earth Elements NSRDS-NBS 60*, U.S. Department of Commerce, Washington, DC, 1978.

123 H. M. Crosswhite, H. Crosswhite, W. T. Carnall and A. P. Paszek, *J. Chem. Phys.*, 1980, **72**, 5103–5117.

124 T. R. Cundari and W. J. Stevens, *J. Chem. Phys.*, 1993, **98**, 5555–5565.

125 V. Vetere, P. Maldivi and C. Adamo, *J. Comput. Chem.*, 2003, **24**, 850–858.

126 M. Atanasov, C. Daul, H. U. Gudel, T. A. Wesolowski and M. Zbiri, *Inorg. Chem.*, 2005, **44**, 2954–2963.

127 W. W. Lukens, N. M. Edelstein, N. Magnani, T. W. Hayton, S. Fortier and L. A. Seaman, *J. Am. Chem. Soc.*, 2013, **135**, 10742–10754.

128 G. J. P. Deblonde, M. Sturzbecher-Hoehne, P. B. Rupert, D. D. An, M. C. Illy, C. Y. Ralston, J. Brabec, W. A. de Jong, R. K. Strong and R. J. Abergel, *Nat. Chem.*, 2017, **9**, 843–849.

129 M. P. Kelley, G. J. P. Deblonde, J. Su, C. H. Booth, R. J. Abergel, E. R. Batista and P. Yang, *Inorg. Chem.*, 2018, **57**, 5352–5363.

130 F. Gendron, V. E. Fleischauer, T. J. Duignan, B. L. Scott, M. W. Löble, S. K. Cary, S. A. Kozimor, H. Bolvin, M. L. Neidig and J. Autschbach, *Phys. Chem. Chem. Phys.*, 2017, **19**, 17300–17313.

131 A. M. Tondreau, T. J. Duignan, B. W. Stein, V. E. Fleischauer, J. Autschbach, E. R. Batista, J. M. Boncella, M. G. Ferrier, S. A. Kozimor, V. Mocko, M. L. Neidig, S. K. Cary and P. Yang, *Inorg. Chem.*, 2018, **57**, 8106–8115.

132 M. B. Jones, A. J. Gaunt, J. C. Gordon, N. Kaltsoyannis, M. P. Neu and B. L. Scott, *Chem. Sci.*, 2013, **4**, 1189–1203.

133 D. D. Schnaars, A. J. Gaunt, T. W. Hayton, M. B. Jones, I. Kirker, N. Kaltsoyannis, I. May, S. D. Reilly, B. L. Scott and G. Wu, *Inorg. Chem.*, 2012, **51**, 8557–8566.

134 E. Lu, S. Sajjad, V. E. J. Berryman, A. J. Woole, N. Kaltsoyannis and S. T. Liddle, *Nat. Commun.*, 2019, **10**, 634.

135 J. Su, E. R. Batista, K. S. Boland, S. E. Bone, J. A. Bradley, S. K. Cary, D. L. Clark, S. D. Conradson, A. S. Ditter, N. Kaltsoyannis, J. M. Keith, A. Kerridge, S. A. Kozimor, M. W. Löble, R. L. Martin, S. G. Minasian, V. Mocko, H. S. La Pierre, G. T. Seidler, D. K. Shuh, M. P. Wilkerson, L. E. Wolfsberg and P. Yang, *J. Am. Chem. Soc.*, 2018, **140**, 17977–17984.

136 H. S. La Pierre and K. Meyer, *Inorg. Chem.*, 2013, **52**, 529–539.

137 H. S. La Pierre, M. Rosenzweig, B. Kosog, C. Hauser, F. W. Heinemann, S. T. Liddle and K. Meyer, *Chem. Commun.*, 2015, **51**, 16671–16674.

138 N. Barros, D. Maynau, L. Maron, O. Eisenstein, G. Zi and R. A. Andersen, *Organometallics*, 2007, **26**, 5059.

139 P. L. Arnold, Z. R. Turner, N. Kaltsoyannis, P. Pelekanaki, R. M. Bellabarba and R. P. Tooze, *Chem.-Eur. J.*, 2010, **16**, 9623–9629.

140 M. Gregson, E. Lu, F. Tuna, E. J. L. McInnes, C. Hennig, A. C. Scheinost, J. McMaster, W. Lewis, A. J. Blake, A. Kerridge and S. T. Liddle, *Chem. Sci.*, 2016, **7**, 3286–3297.

141 A. Streitwieser and U. Mueller-Westerhoff, *J. Am. Chem. Soc.*, 1968, **90**, 7364.

142 R. M. Moore, PhD dissertation, University of California, 1985.

143 W. R. Roth, *Ann. Chem.*, 1964, **671**, 25–31.

144 R. P. Kelly, L. Maron, R. Scopelliti and M. Mazzanti, *Angew. Chem., Int. Ed.*, 2017, **56**, 15663–15666.

145 N. H. Anderson, J. Xie, D. Ray, M. Zeller, L. Gagliardi and S. C. Bart, *Nat. Chem.*, 2017, **9**, 850–855.

146 M. E. Fieser, C. T. Palumbo, H. S. La Pierre, D. P. Halter, V. K. Voora, J. W. Ziller, F. Furche, K. Meyer and W. J. Evans, *Chem. Sci.*, 2017, **8**, 7424–7433.

147 J. Hummer, F. W. Heinemann and K. Meyer, *Inorg. Chem.*, 2017, **56**, 3201–3206.

148 S. S. Galley, A. A. Arico, T. H. Lee, X. Y. Deng, Y. X. Yao, J. M. Sperling, V. Proust, J. S. Storbeck, V. Dobrosavljevic, J. N. Neu, T. Siegrist, R. E. Baumbach, T. E. Albrecht



Schmitt, N. Kaltsoyannis and N. Lanata, *J. Am. Chem. Soc.*, 2018, **140**, 1674–1685.

149 D. N. Huh, J. W. Ziller and W. J. Evans, *Inorg. Chem.*, 2018, **57**, 11809–11814.

150 S. S. Galley, S. A. Pattenaud, C. A. Gaggioli, Y. S. Qiao, J. M. Sperling, M. Zeller, S. Pakhira, J. L. Mendoza-Cortes, E. J. Schelter, T. E. Albrecht-Schmitt, L. Gagliardi and S. C. Bart, *J. Am. Chem. Soc.*, 2019, **141**, 2356–2366.

151 Y. S. Qiao and E. J. Schelter, *Acc. Chem. Res.*, 2018, **51**, 2926–2936.

152 T. C. Weng, G. S. Waldo and J. E. Penner-Hahn, *J. Synchrotron Radiat.*, 2005, **12**, 506–510.

153 A. D. Becke, *J. Chem. Phys.*, 1993, **98**, 5648–5652.

154 C. T. Lee, W. T. Yang and R. G. Parr, *Phys. Rev. B: Condens. Matter Mater. Phys.*, 1988, **37**, 785–789.

155 M. J. Frisch, G. W. Trucks, H. B. Schlegel, G. E. Scuseria, M. A. Robb, J. R. Cheeseman, G. Scalmani, V. Barone, B. Mennucci, G. A. Petersson, H. Nakatsuji, M. Caricato, X. Li, H. P. Hratchian, A. F. Izmaylov, J. Bloino, G. Zheng, J. L. Sonnenberg, M. Hada, M. Ehara, K. Toyota, R. Fukuda, J. Hasegawa, M. Ishida, T. Nakajima, Y. Honda, O. Kitao, H. Nakai, T. Vreven, J. A. Montgomery Jr, J. E. Peralta, F. Ogliaro, M. Bearpark, J. J. Heyd, E. Brothers, K. N. Kudin, V. N. Staroverov, R. Kobayashi, J. Normand, K. Raghavachari, A. Rendell, J. C. Burant, S. S. Iyengar, J. Tomasi, M. Cossi, N. Rega, N. J. Millam, M. Klene, J. E. Knox, J. B. Cross, V. Bakken, C. Adamo, J. Jaramillo, R. Gomperts, R. E. Stratmann, O. Yazayev, A. J. Austin, R. Cammi, C. Pomelli, J. W. Ochterski, R. L. Martin, K. Morokuma, V. G. Zakrzewski, G. A. Voth, P. Salvador, J. J. Dannenberg, S. Dapprich, A. D. Daniels, Ö. Farkas, J. B. Foresman, J. V. Ortiz, J. Cioslowski and D. J. Fox, Gaussian, Inc., Wallingford, CT, 2009.

156 P. Fuentealba, H. Preuss, H. Stoll and L. Vonszentpaly, *Chem. Phys. Lett.*, 1982, **89**, 418–422.

157 W. Küchle, M. Dolg, H. Stoll and H. Preuss, *Mol. Phys.*, 1991, **74**, 1245–1263.

158 W. Küchle, M. Dolg, H. Stoll and H. Preuss, *J. Chem. Phys.*, 1994, **100**, 7535–7542.

159 G. A. Petersson and M. A. Allaham, *J. Chem. Phys.*, 1991, **94**, 6081–6090.

